Title
Fiber-optic-bundle-based optical coherence tomography.

Journal
Optics Letters, 30(14)

ISSN
0146-9592

Authors
Xie, Tuqiang
Mukai, David
Guo, Shuguang
et al.

Publication Date
2005-07-15

DOI
10.1364/ol.30.001803

Fiber-optic-bundle-based optical coherence tomography

Tuqiang Xie, David Mukai, Shuguang Guo, Matthew Brenner, and Zhongping Chen

Beckman Laser Institute, Department of Biomedical Engineering, Pulmonary and Critical Care Division, UC Irvine Medical Center, University of California, Irvine, Irvine, California 92612

Received March 1, 2005

A fiber-optic-bundle-based optical coherence tomography (OCT) probe method is presented. The experimental results demonstrate this multimode optical fiber-bundle-based OCT system can achieve a lateral resolution of 12 μm and an axial resolution of 10 μm with a superluminescent diode source. This novel OCT imaging approach eliminates any moving parts in the probe and has a primary advantage for use in extremely compact and safe OCT endoscopes for imaging internal organs and great potential to be combined with confocal endoscopic microscopy. © 2005 Optical Society of America

OCIS codes: 110.4500, 060.2310, 170.3880, 110.0110, 170.2150.

As a novel noninvasive imaging technique, optical coherence tomography (OCT) provides high-resolution morphological, structural, and functional information in biological tissues.[1] Other noninvasive morphological imaging techniques such as x-ray radiography, magnetic resonance imaging (MRI), computed tomography (CT), and ultrasound imaging have been widely used in various clinical applications with resolutions ranging from 100 μm to 1 mm. However, this resolution is insufficient to delineate the microstructure of biological tissues at the level required to detect abnormalities such as early cancers. OCT can achieve an ultrahigh-resolution as high as 1 μm in real time *in situ* without specimen removal and processing,[2] making it highly attractive for clinical imaging. Since it was first introduced in 1991, OCT has been used to identify microstructures in ophthalmology, the skin, oral cavity, respiratory tract, gastrointestinal tract, and bladder.[3–5] In recent reports, OCT endoscopic and catheter-based probes were developed for clinical use.[6,7] To image tissues, movable parts such as microelectromechanical systems (MEMS) mirrors,[5] MEMS micromotors,[7] linear motors, or rotary fiber joints[8] are used to perform two-dimensional imaging or circumferential scanning. Since the mirror size and numerical aperture are limited by the endoscope size, the lateral resolution is subsequently restricted. Three-dimensional scanning can be accomplished by repeating the scans with an added directional motion component, but this may be technically challenging (particularly precisely aligning components) in small-diameter endoscopic probes. In the confined spaces of endoscopic probes, the sweep distances obtainable with MEMS probes may also be quite limited.

In this Letter we present a new fiber-bundle OCT imaging method with front-view scanning that consists of a fused coherent fiber bundle and an objective lens system. In this system, the scanning mechanism is placed at the proximal fiber-bundle entrance. The bundle, made up of several thousand cores, preserves the spatial relationship between the entrance and the output of the bundle. Therefore, one- or two-directional scanning can be readily performed on the proximal bundle surface to create 2D or 3D images. Because of this fiber-bundle design, the scanning mechanism can be placed proximally and no moving parts or driving current are needed within the endoscope. This design is extremely compact, solid, and reliable and could be modified for required sizes to perform 3D endoscopic imaging in a range of clinical settings.

A schematic of the fiber-bundle-based time-delay superluminescent diode (SLD) OCT system used is shown in Fig. 1. In this case, a SLD with a central wavelength of 1310 nm and a half-maximum full-width (HMFW) spectral bandwidth of 80 nm was used for illumination. The pigtailed output was 10 mW of this source. The axial resolution (Δz) of the OCT system is governed by the coherence length of the light source $(2 \ln 2/\pi)(\bar{\lambda}^2/\Delta\lambda)$ and was approximately 9.5 μm. The light is split into reference and sample arms by a fiber-optic coupler. In the reference arm of a fiber-optic Michelson interferometer, an electro-optic (E-O) phase modulator was inserted into the reference arm before rapid-scanning optical delay

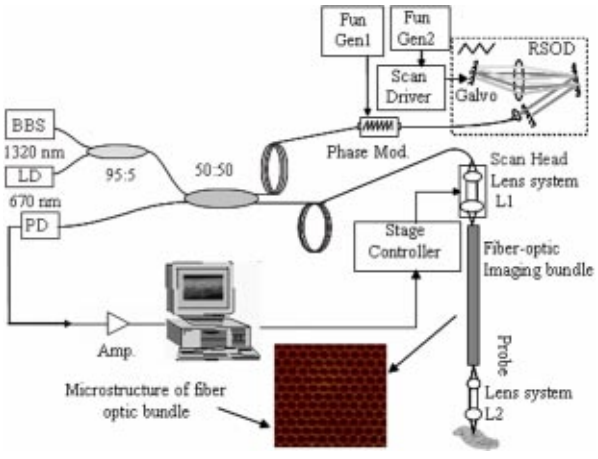

Fig. 1. Schematic of the OCT system based on a coherent fiber bundle and the microstructure of the fiber-optic bundle. BBS, broadband light source; LD, aiming laser diode; PD, photodiode; Fun Gen1, Fun Gen2, function generators.

0146-9592/05/141803-3/$15.00

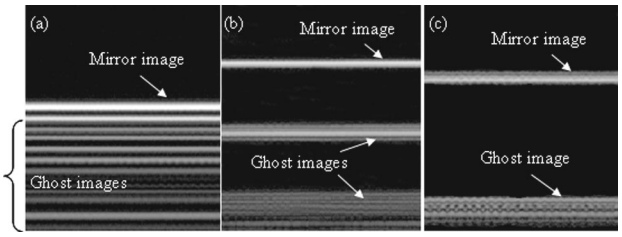

Fig. 2. OCT image of a mirror obtained by the OCT system with different fiber-bundle lengths: (a) 25.4 mm, (b) 152 mm, and (c) 305 mm, with an imaging size of 3 mm by 2.8 mm.

(RSOD). In RSOD, a scanning mirror mounted on a galvanometer was set to zero offset to produce a group delay, and the E-O modulator provided a stable carrier frequency at 500 kHz for the detection of the OCT signal amplitude.

In the sample arm, the light from the single-mode sample fiber was collimated to a Gaussian beam and focused by an objective lens (20×) to a 10 μm beam spot on the proximal entrance plane of the fiber bundle, which was placed at the focal plane of the objective lens. The light beam spot driven by a microstage was laterally scanned on the entrance plane of the fiber bundle. The light emerging from the single fiber cores at the distal end face of the fiber bundle was collimated by an achromatic doublet lens and refocused onto the sample by another achromatic doublet lens. Since the fiber bundle is coherent, the individual fibers preserve their relative spatial relationship as the refocused light beam laterally scans the sample corresponding to the same individual fiber scanning position on the proximal entrance of the fiber bundle.

The fiber bundles used in this study were high-resolution coherent imaging conduits (Schott North America, Massachusetts), each 3.2 mm in diameter, and were studied in varying lengths (25.4, 152, and 305 mm). The fiber bundle is composed of 50,419 individual fiber cores and the external diameter of each individual clad fiber element is 12 μm. The individual fiber core, with a diameter of 9 μm, has a refractive index of 1.58 and a cladding refractive index of 1.48. The numerical aperture (NA) of an individual fiber is 0.55, which is higher than the NA of conventional single-mode fiber (0.22). An important quantity in determining which modes of an electromagnetic field will be supported by a fiber is the characteristic waveguide parameter or the normalized wavenumber (V). The V number of fiber is calculated by

$$V = \frac{\pi \cdot d \cdot NA}{\lambda}, \tag{1}$$

where λ is the wavelength of light and d is the diameter of the fiber core. For our fiber bundle, the V number of the fiber in the bundle is 13.2 for 1300 nm light and much greater than 2.405, which is the maximum V number of fiber supporting only a single mode. This means that a large number of modes including the fundamental mode will be supported by the fiber. Since the input beam NA of 0.28 (of the objective lens) to the fiber bundle is less than the individual fiber NA of 0.55, only low-order modes are coupled into and propagate in the individual fibers avoiding the dispersive effect from high-order modes. To prevent reflection from the end surfaces of the fiber bundle from overwhelming the signal, it is necessary to polish the fiber-bundle end surfaces at an angle (of 8°). This results in near elimination of the reflections at these sites. The transverse magnification ($M_{\text{objective}}$) of lens system L2 in Fig. 1 and the fibers' center-to-center spacing (Δd) in the fiber bundle determine the lateral resolution (Δr), which can be estimated by

$$\Delta r = \frac{\Delta d}{M_{\text{objective}}}. \tag{2}$$

In our setup, the fibers' center-to-center spacing within the fiber bundle is 12 μm and the transverse magnification is close to 1 so that the lateral resolution is approximately 12 μm.

Fiber-bundle lengths of 25.4, 152, and 305 mm were used to obtain the OCT images shown in Figs. 2(a)–2(c), respectively. Ghost images can be seen in these figures. The distance between the fundamental-mode light image and the ghost images, which are produced by other modes, is proportional to the fiber-bundle length. The ghost images from top to bottom become weaker in intensity, and a more dispersive effect is seen. When the bundle length reaches 305 mm, there is one remaining ghost image within the imaging depth range of 2.8 mm, and the fundamental image depth can be more than 1 mm without interruption by the interfering ghost image. If the bundle length is more than 900 mm, the ghost image is out of the display range, and the imaging depth in the fiber-bundle OCT system can be 2.8 mm (the standard depth range of conventional tissue OCT systems) without ghosts. Because the diameter of the individual optical fibers is 10 μm, close to the diameter of normal single-mode fiber (8 μm) for 1300 nm light, the fundamental mode propagates in the multimode fibers of the fiber bundle without extra dispersion as it does in normal single-mode fibers. In the OCT image from the fundamental mode in the fiber, the dispersion could almost be compensated as shown in Fig. 3(b) and the resultant axial resolution

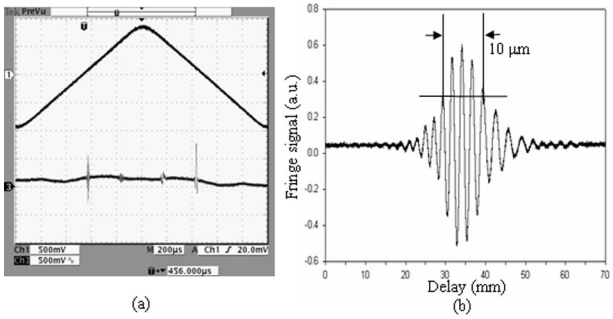

Fig. 3. Interference fringe signal on the (a) time domain and (b) space domain.

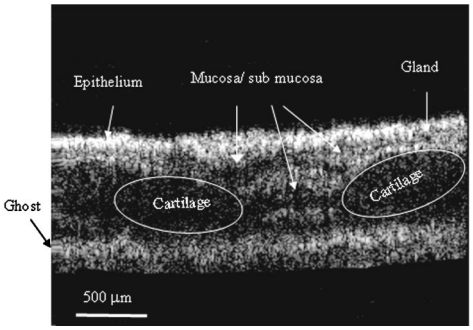

Fig. 4. Two-dimensional OCT image of a fresh rabbit trachea from a fiber bundle OCT system. The image size is 2.8 mm × 2.8 mm. Trachea morphology such as mucosa, submucosa, glands, and cartilage can be seen.

is around 10 μm, which is close to the coherence length of the light source (9.5 μm). During the dispersive compensation, the dispersion of the main interference fringe in the fiber-bundle OCT system was compensated by the grating moving in RSOD as it did in a single-mode fiber OCT system.

A section of normal fresh trachea was excised from a euthanized rabbit and pinned onto a silicone pad. The sample was scanned by the fiber-bundle OCT system and the image shown in Fig. 4 was obtained. The OCT image can delineate the micromorphology of the normal rabbit trachea, including mucosa, submucosa, glands, and cartilage rings, as seen in Fig. 4. Compared to the OCT image from our benchtop OCT system, the fiber-bundle image fidelity, including the signal-to-noise ratio, image depth, and contrast, is slightly degraded. The image quality degradation may be due to coupling loss between the scanning fiber and the fiber bundle. When the focusing beam falls between fiber elements during the lateral scanning beam sweep, the coupling of energy into more than one fiber and into the cladding structure results in a coupling loss that degrades the lateral resolution of the fiber bundle OCT system. Therefore, the image quality can be significantly improved by minimizing the focusing beam size so that the beam size is less than the individual fiber core size, and better coupling of the input beam to each individual fiber core is achieved during scanning.

Since our fiber bundle was fine polished for the angle of 8° on each end, the length differences of individual fibers in the fiber bundle are close to the coherence length of the light source and it is not necessary to reconstruct the OCT image. When the length differences of individual fibers are ΔL, the light path difference is $2\Delta n \Delta L$ for the same axial objective position, where Δn is the refractive-index difference between the fiber core ($n_{\text{glass}} \cong 1.5$) and air ($n_{\text{air}} \cong 1$) and the typical value of $2\Delta n$ is close to 1. If ΔL is longer than the coherence length of the light source, the OCT image should be reconstructed in the image processing software based on the OCT image of a mirror to cancel the effect of the length differences on imaging.

To improve the imaging fidelity, the coupling efficiency can be increased by a number of means including matching the NA between focusing lens system L1 and the bundle, as well as optimizing the lens systems and matching the index between optical component connections. In addition, a specially designed fiber coupler, such as a 90:10 splitting coupler and circulator, could be used in the system to deliver more power to the sample arm from the light source. If two proper gradient-index lenses replace the two achromatic doublet lenses, the probe diameter can be made smaller than 1 mm and will be more solid and easier to pack and seal than the present OCT probes.

In summary, we have described a novel OCT system based on a coherent fiber-optic imaging bundle and demonstrated its feasibility to image biological tissue at transverse and axial resolution of approximately 12 and 10 μm, respectively. Although the fiber bundle consists of multimode fibers, due to large differences between the core index and the cladding index, the fiber bundle can still be used in the sample arm of the OCT system. Enough imaging depth can be achieved to avoid the ghost images from high-order modes when the fiber bundle is long enough. Since the actual scanning mechanism is placed at the proximal entrance of the fiber bundle, it permits simplified two-directional scanning. This approach allows the production of a probe that can be safe without any driving current and extremely compact and solid without any moving parts. This novel fiber-bundle-based OCT system demonstrates the great potential for a high-performance OCT endoscope to image various internal organs in two or three dimensions. This OCT system would be easy to combine with confocal endoscopic microscopy.

This work was supported by the DOD (FA 9550-04-1-0101) and Philip Morris (USA-32598). The National Science Foundation (BES-86924), the National Institutes of Health (EB-00293, NCI-91717, and RR-01192), and the Beckman Laser Institute Endowment are also gratefully acknowledged. T. Xie's e-mail address is txie@uci.edu.

References

1. D. Huang, E. A. Swanson, C. P. Lin, J. S. Schuman, W. G. Stinson, W. Chang, M. R. Hee, T. Flotte, K. Gregory, C. A. Puliafito, and J. G. Fujimoto, Science **254**, 1178 (1991).
2. G. J. Tearney, M. E. Brezinski, B. E. Bouma, S. A. Boppart, C. Pitris, J. F. Southern, and J. G. Fujimoto, Science **276**, 2037 (1997).
3. F. I. Feldchtein, G. V. Gelikonov, V. M. Gelikonov, R. V. Kuranov, and A. M. Sergeev, Opt. Express **3**, 257 (1998).
4. A. M. Rollins, R. Ung-arunyawee, A. Chak, C. K. Wong, K. Kobayashi, M. V. Sivak, and J. A. Izatt, Opt. Lett. **24**, 1358 (1999).
5. T. Xie, H. Xie, G. K. Fedder, and Y. Pan, Electron. Lett. **39**, 1535 (2003).
6. X. Li, C. Chudoba, T. Ko, C. Pitris, and J. G. Fujimoto, Opt. Lett. **25**, 1520 (2000).
7. P. H. Tran, D. Mukai, M. Brenner, and Z. Chen, Opt. Lett. **29**, 1236 (2004).
8. P. Herz, Y. Chen, A. Aguirre, J. G. Fujimoto, H. Mashimo, J. Schmitt, A. Goodnow, and C. Petersen, Opt. Express **12**, 3532 (2004).